First-principles prediction of the morphology of $L1_0$ FePt nanoparticles supported on Mg(Ti)O for heat-assisted magnetic recording applications

Shih-Hsuan Hung* and Keith McKenna†
Department of Physics, University of York, Heslington, York YO10 5DD, United Kingdom
(Received 15 March 2017; revised manuscript received 16 June 2017; published 12 July 2017)

We perform first-principles calculations to predict the morphology of $L1_0$ ordered FePt nanoparticles grown on Mg(Ti)O substrates with relevance to application in heat-assisted magnetic recording (HAMR) media. We show how incorporation of Ti into MgO substrates reduces the FePt adhesion energy from −1.29 (pure MgO) to −2.35 J/m^2 (pure TiO). This effect is due to the formation of strong Fe-Ti bonds at the interface. Consistent with experimental observations, the predicted equilibrium morphology of supported FePt nanoparticles is significantly changed, corresponding to increased wetting. This behavior is undesirable for HAMR media since it promotes grain growth which limits the storage density. We show how passivation of surface Ti atoms (e.g., with MgO) is sufficient to restore the wetting observed for pure MgO substrates offering a viable strategy for optimization of next generation recording media.

DOI: 10.1103/PhysRevMaterials.1.024405

I. INTRODUCTION

$L1_0$ ordered FePt exhibits high magnetrocrystalline anisotropy in the [001] direction (7×10^7 ergs/cm^3) and is one of the preferred materials for heat-assisted magnetic recording (HAMR) media in hard disk drives (HDDs) [1,2]. Increasing the storage density of HDDs further requires decreasing the physical dimensions of each bit which are currently limited by the FePt grain size [3]. $L1_0$ ordered granular FePt has been successfully deposited on (001) MgO underlayers with good (001) texture and large out-of-plane coercivity [3–6]. However, since MgO is insulating, it must be deposited using radio frequency (rf) sputtering which limits the sputtering rate and is impractical for industrial applications. Recent work has shown that rock-salt structured $Mg_{0.2}Ti_{0.8}O$ (MgTiO) can be produced by doping Ti into the MgO substrate [3,7]. Due to the good conductivity of MgTiO, this substrate is suitable for direct current (dc) sputtering which offers better control of the deposition rate and the FePt grain size. However, the shapes of FePt nanoparticles grown on MgTiO are significantly different to those grown on pure MgO. In particular, the contact angle is smaller on MgTiO than on MgO substrates [7]. The increased wetting of FePt on MgTiO makes further reduction of grain size difficult and offsets any benefit obtained by the use of dc sputtering. However, the atomistic origin of the increased wetting on MgTiO is not understood, presenting an obstacle to further optimization of FePt/MgTiO HAMR media.

Experimentally there has been a great deal of effort focused on the development of improved substrates for FePt media. While MgO single crystals are known to provide an ideal substrate for growth of $L1_0$ ordered FePt, they are too expensive for HAMR media applications [8]. Therefore much work has focused on the identification of suitable seed layers that can be grown on silicon substrates to template the growth of $L1_0$ ordered FePt. A thin film of MgO is a natural choice and numerous studies have demonstrated good (001) FePt texture and high coercivity for such films [3–6]. High-resolution transmission electron microscopy studies have also shown that $L1_0$ FePt nanoparticles grow epitaxially on MgO seed layers [9]. However, as noted above, the insulating nature of MgO brings significant disadvantages for industrial applications. The recent work on MgTiO as an alternative conductive seed layer opens up new possibilities [3,7]. However, there is currently very little experimental information concerning the atomic structure at the FePt/MgTiO.

Theoretically, there have also been many investigations into the structure and properties of FePt with relevance to HAMR media. These include first-principles predictions of the stability of FePt surfaces and nanoparticle morphologies [10], as well as Monte Carlo simulations of the ordering of FePt nanoparticles [11,12]. There are far fewer theoretical studies of FePt/MgO interfaces and no results we are aware of concerning the predicted morphology of supported FePt nanoparticles [13,14]. These theoretical models predict that the most stable FePt/MgO interface involves Fe atoms positioned directly above O atoms in the MgO substrate (being around 0.4 eV more stable than the Pt-O configuration) [13]. However, there have been no theoretical studies of the effects of incorporating Ti into MgO on either the interfacial structure or the FePt nanoparticle morphology. Given the absence of direct experimental information on this issue, such predictions would be extremely valuable.

In this study we employ first-principles theoretical approaches to model the interface between $L1_0$ FePt and MgTiO. We show the adhesion of FePt on MgTiO is significantly stronger than on MgO due to the formation of interfacial Fe-Ti bonds. Furthermore, by calculating the surface formation energies of $L1_0$ ordered FePt and applying the Wulff-Kaishew construction we predict the morphologies of FePt nanoparticles on MgTiO substrates with various Ti loadings. These models allow us to provide an atomistic interpretation for the experimentally observed increased wetting of granular FePt on MgTiO. The results also suggest that to reduce the wetting of FePt on MgTiO, interfacial Ti ions must be passivated. This could be achieved for example by introducing an ultrathin pure MgO layer between FePt and the MgTiO substrate. Altogether,

*sh1635@york.ac.uk
†keith.mckenna@york.ac.uk

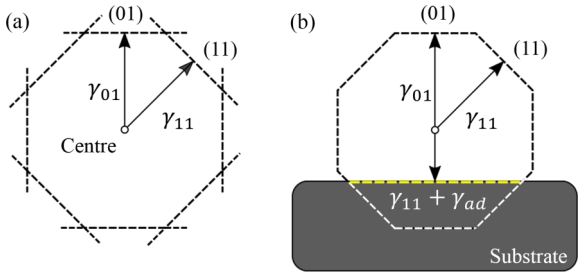

FIG. 1. (a) An illustration of Wulff construction in two dimensions. Vectors corresponding to all low index miller indices are drawn with length proportional to their respective surface formation energy (e.g., as shown above for 01 and 11 surfaces). Lines (planes in 3D) are then drawn representing the surfaces intersecting the tips of these vectors (black dashed lines). The shape enclosed by these surfaces is the one that minimizes the total energy. (b) The Wulff-Kaichew constructions considers that one of the surfaces is in contact with a substrate and so the length of the vector corresponding to this direction is replaced by $\gamma + \gamma_{\text{ad}}$.

these results provide much needed insight into the modified morphology of FePt on MgTiO substrates with direct relevance for the optimization of FePt HAMR media.

II. METHODS

Density functional theory calculations are carried out using the Perdew, Burke, and Ernzerhof (PBE) exchange-correlation potential and a plane wave basis as implemented in the Cambridge Serial Total Energy Package (CASTEP) [15,16]. The Brillouin zone (BZ) is sampled using Monkhorst-Pack (MP) grid (grid sizes for particular supercells are defined later in text) and plane waves with energies up to 500 eV are used to expand the wave functions. The psuedopotentials include the following valence electrons: O ($2s^2 2p^4$), Mg ($s^2 2p^6 3s^2$), Ti ($3s^2 3p^6 3d^2 4s^2$), Fe ($3d^6 4s^2$), and Pt ($4f^{14} 5s^2 5p^6 5d^9 6s^1$). The atomic structure of all supercells presented in this paper are optimized using the limited memory Broyden-Fletcher-Goldfarb-Shanno algorithm [17] with force and energy tolerances of 5×10^{-2} eV/Å and 2×10^{-5} eV/atom, respectively. The energy tolerance for self-consistent field optimisation is 1×10^{-5} eV/atom. We use primitive unit cells for the optimization of bulk FePt and MgO with $9 \times 9 \times 9$ and $13 \times 13 \times 13$ MP grids used for BZ sampling. Using this approach we predict bulk lattice parameters of MgO ($a = 4.25$ Å) and $L1_0$ FePt ($a = 3.83$ Å) in good agreement with experiment [18,19].

The Wulff construction [20] (and its extension to supported nanoparticles: the Wulff-Kaichew construction [21]) is used to predict the equilibrium shape of FePt nanoparticles. These geometric constructions allow one to identify the nanoparticle shape that minimizes the total energy (i.e., the one that is most stable) given surface formation energies (γ) and the adhesion energy if supported on a substrate (γ_{ad}). The basic concept is illustrated in two dimensions in Fig. 1. The Wulff-Kaichew construction is widely used for predicting the morphology of supported nanoparticles, see for instance a recent study of Ag clusters supported on the MgO(100) substrate [22].

To calculate FePt surface formation energies we construct surface slab models (i.e., supercells with periodic boundary conditions parallel to the surface and a vacuum gap in the perpendicular direction separating two equivalent surfaces). The formation energy is then calculated in the following way:

$$\gamma = \frac{1}{2A}(E_{\text{tot}} - N_{\text{FePt}}\mu_{\text{FePt}}), \tag{1}$$

where A is the cross-sectional area of the surface slab, E_{tot} is the total energy of the surface slab, N is the number of FePt formula units in the surface slab, and μ_{FePt} is the chemical potential of bulk FePt (e.g., see Ref. [23]). These calculations are discussed in more detail in Sec. III A below.

To calculate the adhesion energy between FePt and a Mg(Ti)O substrate supercells are constructed containing an interface between a FePt and Mg(Ti)O slab, again with a vacuum gap separating the two free surfaces. The adhesion energy is then calculated in the following way:

$$\gamma_{\text{ad}} = \frac{1}{A}(E_{\text{FePt/Mg(Ti)O}} - E_{\text{FePt}} - E_{\text{Mg(Ti)O}}), \tag{2}$$

where $E_{\text{FePt/Mg(Ti)O}}$ is the total energy of the optimized FePt/Mg(Ti)O interfacial system, and E_{FePt} and $E_{\text{Mg(Ti)O}}$ are the total energies of the optimized FePt and Mg(Ti)O slabs in isolation. Note with this definition a stable interface is characterized by a negative γ_{ad}. These calculations are discussed in more detail in Sec. III C below. We use the VESTA package to construct and visualize the predicted three-dimensional nanoparticle morphologies [24].

III. RESULTS

A. Equilibrium shape of unsupported FePt nanoparticles

In order to predict the equilibrium shape of unsupported FePt NPs we calculate the surface formation energy of the (100), (001), (110), (011), and (111) FePt surfaces using the supercell approach. Each supercell contains a FePt slab with periodic boundary conditions parallel to the surface and a vacuum gap normal to the surface. For all surface supercells the thickness of the slab is at least 10 Å with a vacuum gap of 15 Å. If one constructs a stoichiometric slab with (100), (011), or (111) orientation, the two surface terminations are symmetrically equivalent. However, for a stoichiometric slab with (001) or (110) orientation the two surface terminations are inequivalent (one is Fe terminated, the other is Pt terminated). Therefore, the calculated formation energy of (001) and (110) surfaces represents an average over both Fe and Pt terminations. The (001), (100), (110), (011), and (111) surface slabs contains 20, 20, 8, 10, and 10 atoms, respectively (the supercells used for these calculations are included in the Supplemental Material [25]). $9 \times 9 \times 1$ MP grids are used for the BZ sampling with only 1 k point in the direction normal to the surface. Table I shows the formation energy of the five low-index FePt surfaces calculated using Eq. (1). The results are in very good agreement with previous calculations employing a very similar approach but a different code [10]. The (111) surface, which has the highest coordination, is the most stable ($\gamma_{111} = 1.834$ J/m^2), whereas the (100) surface is the least stable ($\gamma_{100} = 2.196$ J/m^2). The equilibrium crystal shape of FePt predicted using the Wulff construction is a

TABLE I. Surface formation energies for the five low-index surfaces of $L1_0$ FePt together with a comparison to previous first-principles results by Dannenberg *et al.* [10].

Surface formation energy	This work (J/m^2)	Previous work [10] (J/m^2)
(100)	2.196	2.125
(001)	2.195	2.121
(110)	2.153	2.085
(011)	2.100	2.008
(111)	1.834	1.871

truncated octahedron with 14 facets including four (100), two (001), and eight (111) facets (Fig. 2). Figure 2 also shows an atomic model of an unsupported FePt nanoparticle. We note that the atomic model corresponds to perfectly $L1_0$ ordered FePt, whereas in reality disorder and intermixing of Fe and Pt on different surface facets may take place as shown in previous Monte Carlo simulations [11].

B. Incorporation of TiO into the MgO substrate

In order to investigate the wetting of FePt on MgTiO we first need to understand how TiO incorporates into the MgO substrate. While rock-salt TiO is not a thermodynamically stable phase, it can be synthesized as a metastable structure when mixed with MgO [3,7,26]. The calculated lattice constants of rock-salt MgO and TiO are 4.25 and 4.28 Å, respectively. Since the lattice constants differ by less than 1%, doping TiO into MgO is expected to introduce little strain. In order to predict the stable structure of the TiO doped MgO surface, we investigate surface slabs involving different configurations of TiO and MgO. We consider supercells consisting of ten atomic layers (MgO or TiO), a 15 Å vacuum gap normal to the slab surface, and periodic boundary conditions parallel to the surface (using the bulk MgO lattice constant). All of the supercells used for these calculations contain 40 atoms (supercells included in the Supplemental Material [25]) and a

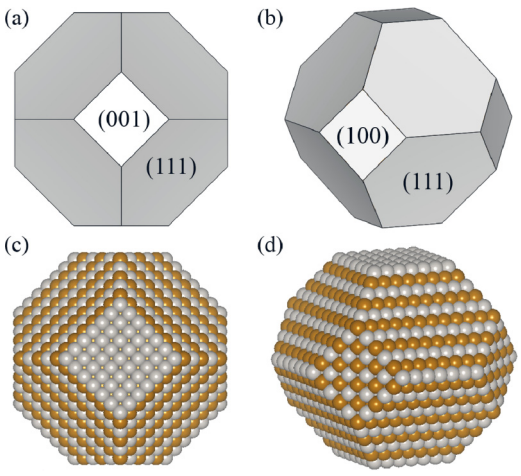

FIG. 2. (a) and (b) Two different views of the FePt morphology predicted to be most stable. (c) and (d) Corresponding illustrative examples of the atomic structure of a FePt nanoparticle. The brass and sliver spheres represent the iron and platinum atoms, respectively.

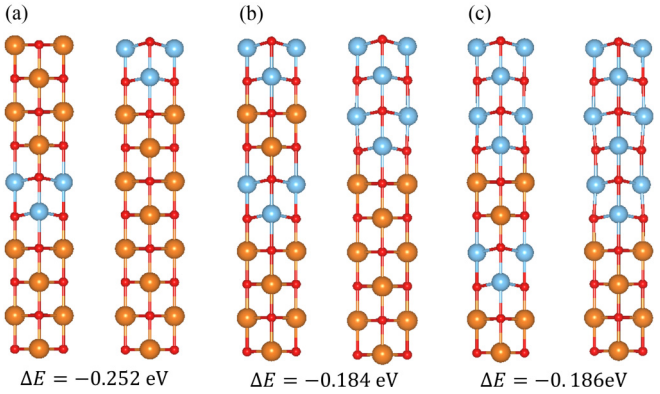

FIG. 3. Different optimized configurations of Ti incorporated into MgO used to assess preferential incorporation sites. (a) 2 monolayers of Ti substituted into the center of a slab (left) and at the surface (right). The latter is found to be more stable ($\Delta E = -0.252$ eV). (b) An additional 2 monolayers of Ti substituted into the slab is again found to be more stable segregated at the surface ($\Delta E = -0.184$ eV). (c) A further 2 monolayers of Ti substituted into the slab is again found to be more stable segregated at the surface ($\Delta E = -0.186$ eV). The red, orange, and blue spheres represent oxygen, magnesium, and titanium atoms, respectively.

$5 \times 5 \times 1$ MP grid is used for BZ sampling. Figure 3 shows the optimized structures of the MgO slab with two, four, and six substitutional TiO layers [hereafter referred to as MgTi(2)O, MgTi(4)O, and MgTi(6)O]. For each case two different TiO arrangements are shown. We note that the TiO layers in the slabs undergo a small ferroelectric distortion normal to the surface (Fig. 3). As a consequence even numbers of TiO layers are found to be much more stable than odd numbers of TiO layers. For MgTi(2)O, MgTi(4)O, and MgTi(6)O in Fig. 3, ΔE gives the difference in total energy between the configuration on the left and the configuration on the right. In all cases the configurations with TiO segregated to the surface are found to be more stable than those with TiO dispersed in the bulk (i.e., ΔE is negative). The calculated electronic density of states for the MgO slabs with TiO at the surface shows a band of metallic states near the Fermi energy suggesting they should exhibit increased conductivity, consistent with experiment.

C. Structure and adhesion energy of FePt/Mg(Ti)O interfaces

In this section we optimize the structure of interfaces between FePt and various Mg(Ti)O substrates and calculate their adhesion energies using Eq. (2). We use the same supercell as in Sec. III B but extended normal to the surface to accommodate ten FePt layers with 60 atoms in total. The supercells for these calculations are also included in the Supplemental Material [25] and we use the same MP grid for sampling as in Sec. III B. Following previous work Fe atoms are positioned in the most stable position above O atoms of the substrate [13]. We verified that adsorption with Fe aligned above Ti atoms is less stable. In this geometry the FePt layers experience 10% in-plane strain. We consider FePt on MgTiO substrates containing between zero and ten TiO layers [MgO, MgTi(2)O, MgTi(4)O, MgTi(6)O, MgTi(8)O, and TiO]. In all cases the TiO layers are segregated to the surface according

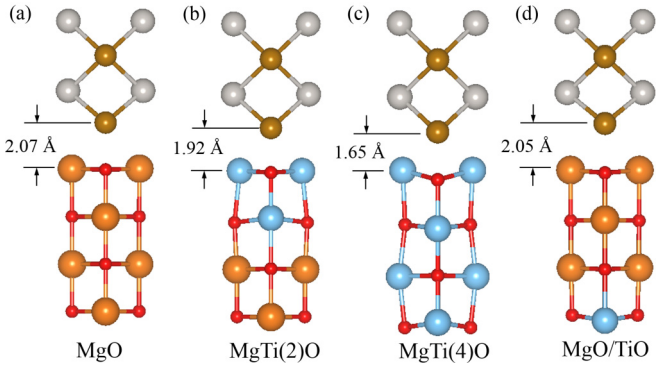

FIG. 4. Optimized atomic structures of FePt/Mg(Ti)O systems [shown in (110) projection] with corresponding vertical distances between the interfacial Fe atom and adjacent cation (Mg or Ti) labeled. (a) FePt/MgO, (b) FePt/MgTi(2)O, and (c) FePt/MgTi(4)O. (d) Optimized atomic structure of FePt supported on a pure TiO slab passivated with 3 monolayer coating of pure MgO. In this case the vertical distance and adhesion energy is similar to that for a pure MgO substrate. The brass, sliver, orange, red, and blue spheres represent the iron, platinum, magnesium, oxygen, and titanium atoms, respectively.

to the results in Sec. III B. Figure 4 shows the optimized interfacial structure of selected FePt/Mg(Ti)O systems and the vertical distance between Fe and either Mg or Ti at the interface. The vertical distance is found to decrease from 2.07 Å (FePt/MgO) to 1.65 Å (FePt/TiO) on increasing the amount of TiO. Figure 5 shows how the adhesion energy varies as the number of TiO layers is increased. The adhesion energy decreases from -1.3 (pure MgO) to around -2.4 J/m^2 for high Ti concentration. The inset in Fig. 5 shows the almost linear correlation between vertical distances and adhesion energies. The results above suggest the attraction between Fe and Ti at the interface reduces the vertical distance and is responsible for a decrease in the adhesion energy.

Analysis of the charge transfer at the Mg(Ti)O/FePt interface provides deeper insight into strengthening of the Fe-Ti bond associated with the decreased adhesion energy.

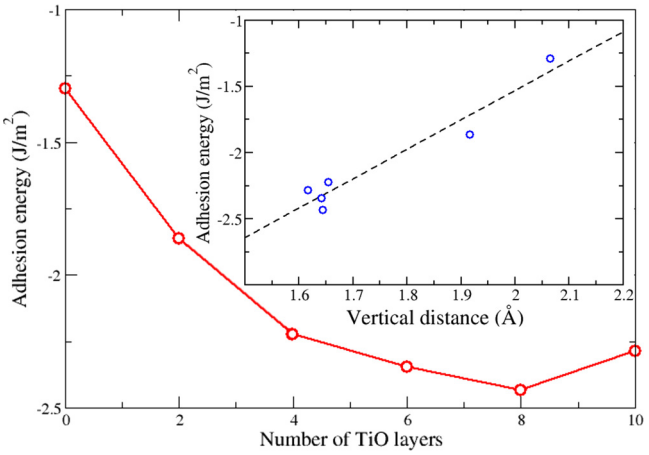

FIG. 5. Variation of adhesion energy with the number of Ti monolayers incorporated into the MgO substrate (red line). The inset shows the positive correlation between the vertical gap (see Fig. 4) and the adhesion energy.

We have performed Bader analysis to calculate the charge associated with each atom in the interface supercells [27]. We then calculate the charge transfer (Δq) with respect to the isolated FePt and Mg(Ti)O slabs for all atoms as a function of the number of TiO layers in the Mg(Ti)O substrate. We find that there is very small charge transfer throughout FePt except for the Fe and Pt atoms directly at the interface. Figure 6 shows how the charge transfer varies with the number of TiO layers in the Mg(Ti)O substrate. We see that as the number of TiO layers increases there is appreciable negative charging of the interfacial Fe accompanied by a positive charging of the adjacent Pt and Mg(Ti)O substrate. For four or more TiO layers approximately 0.4 electrons are transferred to the Fe atom. The majority of this charge comes from the substrate with a smaller contribution from the adjacent Pt atom. Accompanying the charge transfer to Fe is a decrease in the magnetic moment from 3.4 to 3.0 μ_B. The magnetic moment of other Fe atoms away from the interface are not significantly modified. The negative charging of Fe and the corresponding positive charging of the Ti atom in the substrate increases the ionicity of the Fe-Ti bond driving a shortening of the bond length. The local density of states is also modified as a result of this charge transfer (see Fig. S1, Supplementary Material [25]) with new electronic states introduced in the spin down channel in a range 1.0 to 2.5 eV below the Fermi energy associated with the interfacial Fe atoms.

D. Morphology of FePt nanoparticles supported on MgO and MgTiO

Using the results from the previous sections we predict the equilibrium shapes of supported FePt nanoparticles using the Wulff-Kaishew construction (see Sec. II). Figure 7 shows the predicted morphologies and atomic models for FePt supported on the pure MgO substrate and a MgTiO substrate with >4 monolayers of TiO at the surface. The predicted equilibrium shape of FePt supported on MgO is a height-reduced truncated octahedron with a large contact angle at the interface between the FePt $(11\bar{1})$ facet and the MgO (001) surface [Fig. 7(a)]. For FePt supported on a MgTiO substrate the height is reduced further due to the increased adhesion energy. As a result the contact angle [now between the FePt (111) facet and MgO (001) surface] is reduced [Fig. 7(b)]. For both cases we also show representative atomic models in Fig. 7. The above results show that TiO doping in the MgO substrate decreases the FePt adhesion energy and increases the wetting of granular FePt, which hinders the growth of isolated FePt grains. One strategy to overcome this issue is to introduce an intermediate layer between FePt and the substrate to passivate the surface Ti. For example, one could use a thin film of pure MgO on top of TiO doped MgO as a passivation layer. We performed a calculation of the FePt adhesion energy with 3 monolayers of MgO as the passivation layer and find the adhesion energy is increased to -1.23 J/m^2, which is comparable to that of the FePt/MgO system [Fig. 4(d)]. The vertical Fe-Mg distance is also increased to 2.05 Å. Using the increased adhesion energy the equilibrium shape is very similar to the pure MgO case with a large contact angle [Fig. 7(a)]. Therefore, it is confirmed a thin MgO layer has the capability to passivate the Fe-Ti bonds at the interface and reduce the wetting on the MgTiO substrate.

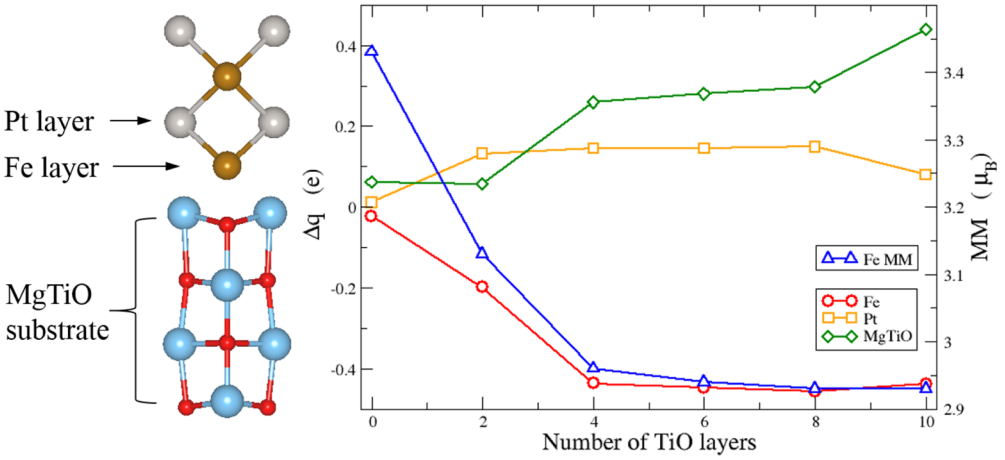

FIG. 6. (Left) A schematic showing an interface supercell with the interfacial Fe and Pt atoms as well as the Mg(Ti)O substrate atoms indicated. (Right) Variation of the charge transfer (Δq, left scale) with number of TiO layers for the interfacial Fe and Pt atoms as well as the Mg(Ti)O substrate. Also shown is the magnetic moment on the interfacial Fe atom (right scale).

IV. DISCUSSION AND CONCLUSIONS

There are several factors that may influence the accuracy of the results presented above. First, FePt is strained by 10% in our calculation. In reality this large lattice mismatch would be partially relieved by formation of dislocations at the interface (e.g., see recent work addressing this issue for the FePt/TiN system [19]). Modeling dislocations at the interface would require a supercell that is about 100 times larger than the one considered here, which is currently computationally prohibitive at the density functional theory level. However, even in the presence of dislocations we expect the interaction between Ti and Fe at the interface would give rise to decreased adhesion energy and increased wetting as elucidated by our calculations. Another issue is that the lattice constant of the MgTiO structures may in general differ from that of MgO. However, the strain we have calculated for TiO is less than 1%, suggesting this should not affect the results significantly. We also note that while the PBE functional is known to underestimate the band gap of many oxides, the total energies should be accurate for calculating adhesion energies and predicting the shape of FePt nanoparticles.

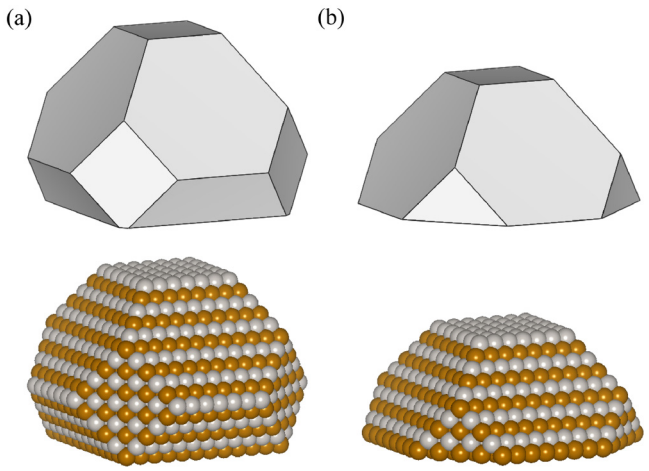

FIG. 7. Predicted morphologies and illustrative atomic structures for FePt nanoparticles supported on (a) pure MgO and (b) MgO with more than 4 monolayers of TiO incorporated at the surface. The brass and sliver spheres represent the iron and platinum atoms, respectively.

As noted in the Introduction there is relatively little experimental information on the atomic structure of the FePt/MgTiO interface with which to compare. The main observation is that the wetting of FePt on MgTiO is significantly stronger than on pure MgO substrates which is fully consistent with our models. Many of the other predictions presented in this article would also be amenable for testing experimentally. For example, the systematic investigation of incorporation of TiO in MgO suggests it should prefer to segregate to the surface which could be probed directly using electron energy loss spectroscopy mapping within a scanning transmission electron microscope (STEM) [28]. We also predict significant displacements of the interfacial Ti at the interface with FePt associated with the formation of Ti-Fe bonds which could be probed directly by STEM. Finally, our prediction that deposition of a 3 monolayer passivating MgO layer on top of MgTiO should be sufficient to restore the nanoparticle morphology to that found on pure MgO would also be straightforward to test experimentally.

In this paper we have focused on understanding how incorporation of Ti into MgO modifies the structure and morphology of supported FePt nanoparticles. However, several alternatives underlayers such as TiN [29,30], TiON [30], and FeCoNi [31] have also been studied and show promise. We note that many of these underlayers also include Ti (or other transition metal elements) and so Fe-Ti bond formation may also play a role in influencing FePt wetting and nanoparticle growth for these systems. In HAMR media it is also necessary to co-sputter FePt with materials such as carbon [32] or SiO_2 [33] which segregate to the nanoparticle surface and form amorphous boundaries, decoupling the grains and promoting the growth of smaller grains. While it is possible these additives may influence the nanoparticle morphology it is not expected they will incorporate at the FePt/MgTiO and so the conclusions regarding the origin of increased wetting should be unchanged.

The magnetic anisotropy energy (MAE) is another very important parameter for applications in HAMR media. In particular, it is important that whatever modifications are

employed to optimize growth processes do not destroy the out-of-plane magnetization exhibited on FePt/MgO. However, calculating the MAE for the systems studied in this paper is challenging and is likely to be sensitive to strain (which is overestimated in our calculations due to the absence of misfit dislocations). Calculation of the MAE would be an interesting next step but is beyond the scope of the present work.

In summary, we have investigated the adhesion energy between FePt and MgTiO using first-principles calculations. We find that Ti incorporated into MgO films prefers to segregate to the surface where it modifies the interaction with FePt through the formation of Fe-Ti bonds. As the Ti content is increased the vertical Fe-Ti distance at the interface is found to contract from 2.07 to 1.65 Å, accompanied by a decrease in the adhesion energy from -1.29 to -2.35 J/m^2. Using the calculated adhesion energies we also predicted the equilibrium shapes of supported FePt nanoparticles using the Wulff-Kaishew construction. The predicted morphology is a height-reduced truncated octahedron with stronger wetting for Ti doped substrates compared to pure MgO substrates. The predicted FePt shapes are in good agreement with experimental cross-sectional transmission electron microscopy images [7]. Although the TiO doping of MgO is attractive as it allows for growth by dc sputtering, the increased wetting hinders the growth of isolated FePt grains. A viable solution to this problem is to passivate the surface Ti, e.g., with a ultrathin MgO or nitride layer. These theoretical predictions provide much needed atomistic insight and point towards viable strategies for the optimization of for HAMR media.

ACKNOWLEDGMENTS

K.P.M. acknowledges support from EPSRC (EP/K003151/1). This work made use of the facilities of Archer, the UK's national high-performance computing service, via our membership in the UK HPC Materials Chemistry Consortium, which is funded by EPSRC (EP/L000202/1). This work also made use of the facilities of N8 HPC Centre of Excellence, provided and funded by the N8 consortium and EPSRC (EP/K000225/1). The Centre is coordinated by the Universities of Leeds and Manchester. The authors also thank Kazuhiro Hono for helpful discussions. All data created during this research are available by request from the University of York Research database http://dx.doi.org/10.15124/6e34c91a-3e04-4cb8-b0e2-efe9b440ce95.

[1] S. N. Piramanayagam, J. Appl. Phys. **102**, 011301 (2007).
[2] S. Khizroev and D. Litvinov, J. Appl. Phys. **95**, 4521 (2004).
[3] K. Hono and Y. Takahashi, *$L1_0$-FePt Granular Films for Heat-Assisted Magnetic Recording Media* (Pan Stanford, Boca Raton, FL, 2016), pp. 245–277.
[4] T. Shima, K. Takanashi, Y. K. Takahashi, and K. Hono, Appl. Phys. Lett. **85**, 2571 (2004).
[5] Y. Peng, J.-G. Zhu, and D. E. Laughlin, J. Appl. Phys. **99**, 08F907 (2006).
[6] A. Perumal, Y. K. Takahashi, T. O. Seki, and K. Hono, Appl. Phys. Lett. **92**, 132508 (2008).
[7] B. S. D. C. S. Varaprasad, Y. K. Takahashi, A. Ajan, and K. Hono, J. Appl. Phys. **113**, 203907 (2013).
[8] J. Wang, S. Hata, Y. K. Takahashi, H. Sepehri-Amin, B. S. D. C. S. Varaprasad, T. Shiroyama, T. Schrefl, and K. Hono, Acta Mater. **91**, 41 (2015).
[9] S. Fukami, A. Ohno, and N. Tanaka, Mater. Trans. **45**, 2012 (2004).
[10] A. Dannenberg, M. E. Gruner, A. Hucht, and P. Entel, Phys. Rev. B **80**, 245438 (2009).
[11] B. Yang, Scr. Mater. **53**, 417 (2005).
[12] M. Müller, P. Erhart, and K. Albe, Phys. Rev. B **76**, 155412 (2007).
[13] W. Zhu, H.-C. Ding, S.-J. Gong, Y. Liu, and C.-G. Duan, J. Phys.: Condens. Matter **25**, 396001 (2013).
[14] R. Cuadrado and R. W. Chantrell, Phys. Rev. B **89**, 094407 (2014).
[15] J. P. Perdew, K. Burke, and M. Ernzerhof, Phys. Rev. Lett. **77**, 3865 (1996).
[16] S. J. Clark, M. D. Segall, C. J. Pickard, P. J. Hasnip, M. I. J. Probert, K. Refson, and M. C. Payne, Z. Kristallogr. **220**, 567 (2005).
[17] R. Fletcher, *Practical Methods of Optimization* (Wiley, New York, 1980).
[18] S. Sasaki, K. Fujino, and Y. Takéuchi, Proc. Jpn. Acad. Ser. B **55**, 43 (1979).
[19] H. H. Li, K. F. Dong, J. F. Hu, T. J. Zhou, G. M. Chow, and J. S. Chen, J. Phys. D: Appl. Phys. **46**, 015002 (2013).
[20] L. D. Marks, Rep. Prog. Phys. **57**, 603 (1994).
[21] P. Müller and R. Kern, Surf. Sci. **457**, 229 (2000).
[22] S. Stankic, R. Cortes-Huerto, N. Crivat, D. Demaille, J. Goniakowski, and J. Jupille, Nanoscale **5**, 2448 (2013).
[23] S. K. Wallace and K. P. Mckenna, J. Phys. Chem. C **119**, 1913 (2015).
[24] K. Momma and F. Izumi, J. Appl. Crystallogr. **44**, 1272 (2011).
[25] See Supplemental Material at http://link.aps.org/supplemental/10.1103/PhysRevMaterials.1.024405 for all supercells in CIF format.
[26] K. Hono (private communication).
[27] G. Henkelman, A. Arnaldsson, and H. Jónsson, Comput. Mater. Sci. **36**, 354 (2006).
[28] Z. Wang, M. Saito, K. P. McKenna, L. Gu, S. Tsukimoto, A. L. Shluger, and Y. Ikuhara, Nature (London) **479**, 380 (2011).
[29] H. H. Li, K. F. Dong, Y. G. Peng, G. Ju, G. M. Chow, and J. S. Chen, J. Appl. Phys. **110**, 043911 (2011).
[30] K. F. Dong, H. H. Li, Y. G. Peng, G. Ju, G. M. Chow, and J. S. Chen, Sci. Rep. **4**, 5607 (2014).
[31] M. L. Yan, X. Z. Li, L. Gao, S. H. Liou, D. J. Sellmyer, R. J. M. Van De Veerdonk, and K. W. Wierman, Appl. Phys. Lett. **83**, 3332 (2003).
[32] H. S. Ko, A. Perumal, and S. C. Shin, Appl. Phys. Lett. **82**, 2311 (2003).
[33] T. O. Seki, Y. K. Takahashi, and K. Hono, J. Appl. Phys. **103**, 023910 (2008).